Journal of Radioanalytical and Nuclear Chemistry (2023) 332:297–310
https://doi.org/10.1007/s10967-022-08723-1

# Magnetite based green bio composite for uranium exclusion from aqueous solution

**Poonam Deshmukh[1] · Santosh Kumar Sar[1] · Manoj Kumar Jindal[1,3] · Tonmoy Ray[2]**

Received: 21 September 2022 / Accepted: 13 December 2022 / Published online: 31 December 2022


## Abstract

The work demonstrates a new greener approach in developing bio-composite magnetic nanoparticles ($Fe_3O_4$@PBP) containing a sorbent extracted from papaya (*Carica papaya*) bark for efficient uranium (VI) sorption from aqueous media. The findings showed that $Fe_3O_4$@PBP nano composites exhibited a characteristic average size of around 26.4 nm, as inferred from the XRD data. Further, these nano composite performed well in the uptake of uranium (VI), revealing the removal efficiency and the maximum adsorption capacity to be 88.8% and 120.48 mg/g, respectively. The thermodynamic investigation indicated that the endothermic uranium(VI) uptake sorption process by expeditious $Fe_3O_4$@PBP nano composite is naturally impulsive.

## Graphic abstract

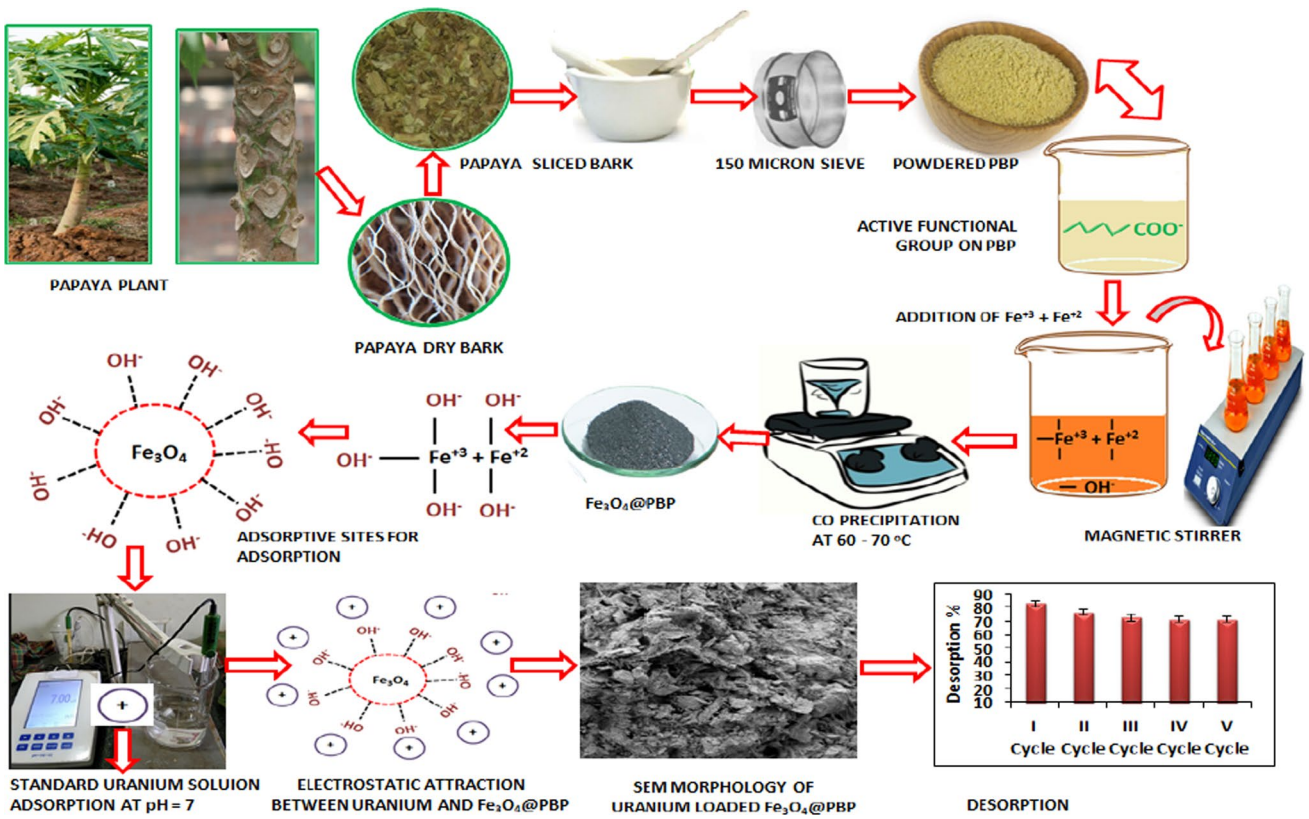


**Keywords** Radionuclide · Magnetite · Remediation · Magnetic nanocomposite · Adsorption

Extended author information available on the last page of the article

## Introduction

In today's technology-driven time, sustainable utilization of natural resources is linked to issues such as reducing pollution, the use of native plants as scavengers of pollutants, and so on. The prevalence of hazardous toxic metals, as a result of fast industrialization and technological advancement, is a global environmental issue. Recently, there has been a boom in interest in the use of biomass from diverse sources to reduce toxic metals from diluted, large-volume solutions. Human beings require a lot of energy as a civilization. Because of the expansion of civilization, the world's energy demand has gone through the roof in the last few decades [1]. Among the different sources of energy, such as sound, light, mechanical, electrical, chemical and nuclear energy; nuclear energy is crucial in the modern period. Uranium is one of the primary basic elements used in nuclear fission for radioactive disintegration [2]. Numerous radioactive isotopes and heavy hazardous metals are discharged into the wastewater from the nuclear reactor during the disintegration process. The high levels of uranium and heavy toxic elements found in the water samples are extremely dangerous to human health and all other living creatures. The WHO recommends that the permissible limit of 30 µg/ L for Uranium in drinking water (World Health Organization) [3]. Uranium ions are discharged into water bodies from various causes such as uranium radioactive waste, mining and geological interaction [4, 5]. Uranium is toxic to the kidneys lungs, and even the neurological system. The formation of complexes with phospholipids and proteins in cells has been ascribed to uranium's adverse effects on the organs. Because of the high uranium concentration, major health risks such as nephrotoxicity and cancer risk may occurs in the body system [6]. To prevent such condition, it is essential to extract uranium and heavy hazardous elements from contaminated water samples. Research teams have currently developed a variety of strategies for removing heavy hazardous metal ions, including bio-reduction [7], reverse osmosis [8], adsorption [9], and precipitation [7]. Adsorption is the most commonly used approach due to its convenience, ease of operation, and able to quickly remove any target toxicant from the medium [10]. However, typical adsorbent materials have some limitations, such as less adsorption potential and higher material development costs. Therefore, researchers are always attempting to produce less expensive, higher potential, and environmentally acceptable sorbents to extract uranium and other heavy hazardous metals from raw water [11]. Iron-loaded biochar [12], alumina [13], iron zirconium oxide [14], and waste materials from agriculture [15] have all been investigated for their ability to adsorb arsenic. For removal of arsenic, maghemite, hematite, and magnetite [16] have been employed at various pH levels along with their minimal cost and local availability. Ion-imprinted magnetic chitosan resins, chitosan powder, calcium alginate beads, tea waste, citrus waste, nano porous and non-nano porous alumina, zeolite NaA, natural white silica sand, magnetite nanoparticle, silica gel with benzylthiourea derivatives, activated carbon prepared from olive stones, chitosin coated attapulgite, wood powder and wheat straw, and activated carbon have also been reported for uranium adsorption [17]. The use of iron oxide papaya bark powder hybrids i.e. $Fe_3O_4$@PBP magnetic bio nanocomposite for uranium removal is a novel method. The papaya bark powder (PBP) provides a porous surface to spread and hold the iron oxide adsorbent, as well as increasing the surface area of the iron oxide. Nanocomposites are easily produced by adding the base to an aqueous $Fe^{2+}$ and $Fe^{3+}$ containing solution. Because these particles rapidly agglomerate, a moderate surface-area carrier, such as PBP, can be used to disperse the particles while maintaining total adsorbent particle sizes suitable for the batch adsorption process [18]. Co-precipitation [19] was used to produce $Fe_3O_4$@PBP magnetic bio nanocomposite as a metal ion adsorbent in this work. $Fe_3O_4$@PBP magnetic bio nanocomposite was made with $Fe_3O_4$ loading and successfully used to remediate uranium-contaminated water in this study. The main objective of the study was to look into the potential of $Fe_3O_4$@PBP as a bio-sorbent in minimizing uranium (VI) concentrations in an aqueous path. *Carica papaya* is the scientific name for papaya, which belongs to the *Caricaceae* family. Papaya is an herbaceous plant with self-supporting stems, not a tree. [20]. The important chemical components of papaya wood are protein (4.41%), crude fiber (32.39%), and mineral ash (6.25%) [21]. Crude fiber contains lignin and cellulose, an indication of the presence of hemicellulose and associated polysaccharides [22]. Magnetic biocomposites are in high demand due to their applicability in a wide range of fields, including medicine antimicrobial agents, biosensors, and recycling techniques [23]. Researchers pay attention to the significant potential of $Fe_3O_4$ particles, such as their magnetic capabilities. $Fe_3O_4$@PBP is used as plant-based magnetic particle with unusual capabilities due to the presence of cations, $Fe^{2+}$ and $Fe^{3+}$, in its crystalline structure. Because of the presence of many functional groups on the surface of bio sorbent, they have the potential to gather and hold pollutants from an aqueous medium [24]. The purpose of this research is to demonstrate and gather information on the potential usage of magnetic adsorbents for the removal of U (VI) from the aqueous phase. This study makes use of the findings of a batch adsorption study that looked at several parameters for U (VI) removal. The main purpose of the research is to assess the potential of magnetic

adsorbents to adsorb metal contaminated water. Green synthesis is significant as it stands as an essential example in the synthesis of $Fe_3O_4$@PBP as an adsorbent that is potentially harmless to humans. After all, the materials used are taken from a natural source, such as plant extract. Plant extracts can act as both stabilizing and reducing agents during the $Fe_3O_4$@PBP synthesis process. This method is not only simple but also inexpensive. To put it into perspective, the green technique is a non-hazardous to the environment or human exposure method of producing magnetic particles. The focus of this research is to develop novel methods for producing magnetic particles using native plants. In current history, research teams have been looking for sustainable ways to make magnetic biocomposites from regenerative waste resources to achieve global demands.

## Materials and methodology

### Required chemicals for analysis

A standard Uranium solution of 1 g/L in distilled water was made using 2.1308 g of $UO_2(NO_3)_2 \cdot 6H_2O$ and Arsenazo III procured of Sigma-Aldrich (USA) make; Merck (India) manufactured tartaric acid (> 99%) and iron (II) sulfate [($FeSO_4 \cdot 7H_2O$) 99%] were used. The DTPE [(diethylenetriaminepentaacetic acid) 99%] and 99% anhydrous ferric chloride ($FeCl_3$) were used of Loba Chemie Pvt. Ltd. India and Molychem make.

### Collection and screening of sample

The sample was gathered from the local area, and the bark was collected from a fallen trunk of a mature plant of papaya (*Carica papaya*). The trunk was debarked, sliced into small pieces, immersed in boiling water for around 45 min, cleaned exhaustively under running water, and placed in distilled water for 3–4 h. Further, the water was changed 2–3 times to eliminate the undesirable particles. This was done to soften the sorbent (*Carica papaya*) [25]. They were oven dried at 40° C till crisp (approx. 48 h). The dried materials were then mashed and sieved using a 150 µm sieve before being used for sorption tests. The papaya bark has a considerable surface area, which is ideal for metal sorption [21]. For trials, the papaya bark powder (PBP) was stored in sterile environment i.e. in a sealed jar.

## Green synthesis of magnetic bio nanocomposite ($Fe_3O_4$@PBP)

A simple method for producing nanoparticles requires only a metal salt (precursor) and a green substrate (Reducing agent). Several parameters including metal salt concentration, green substrate concentration, reaction time, temperature, and solution pH were modified during the nanoparticle synthesis process to get the features desired for different applications. An aqueous solution comprising iron salts and a base (NaOH) was hydrolyzed at room temperature in an ambient environment to produce $Fe_3O_4$. In brief, $Fe_3O_4$@PBP was synthesized by co-precipitating $Fe^{2+}$ and $Fe^{3+}$ in a stociometric ratio on a magnetic stirrer at 60–70 °C for 24 h [19]. In this work, papaya bark powder (PBP) was utilized as a reducing and/or stabilizing agent to assist enough particles to escape the aggregation process and reduce the mean particle size overall. Finally, the $Fe_3O_4$@PBP as a sorbent was filtered and rinsed many times with distilled water, followed by ethanol (until the neutral pH), and finally dried at 50 °C in the oven. A magnetic sample ($Fe_3O_4$@PBP) was isolated using a permanent magnet. The hydroxylation of the $Fe^{2+}$ (ferrous) and $Fe^{3+}$ (ferric) ions results in the formation of $Fe(OH)_2$ and $Fe(OH)_3$ at high pH. When NaOH was added as a precipitant, the precipitate was produced immediately. As a result, black precipitation led to the formation of $Fe_3O_4$ nanoparticles. The reaction is fast, with a high yield, and magnetite ($Fe_3O_4$) crystals appear instantly following the addition of an iron from its salt [26]. The proposed reaction scheme for the synthesis of magnetic particles ($Fe_3O_4$@PBP) is as follows:

1. $Fe^{3+} + 3OH^- \xrightarrow{\text{Hydroxylation}} Fe(OH)_3$
2. $Fe(OH)_3 \rightarrow FeOOH + H_2O$
3. $Fe^{2+} + 2OH^- \xrightarrow{\text{Hydroxylation}} Fe(OH)_2$
4. $2FeOOH + Fe(OH)_2 \rightarrow Fe_3O_4 \downarrow \text{(Black ppt.)} + 2H_2O$
5. $Fe_3O_4 + PBP \rightarrow Fe_3O_4@PBP\ (\text{Magnetic bio} - \text{composite})$

## Instrumentation

EDX (Energy Dispersive X-Ray) and Scanning electron microscopy (FE-SEM) i.e. field emission scanning electron microscope (ZEISS) were used for obtaining the elemental characterization and surface morphology of $Fe_3O_4$@PBP, in the laboratories of IIT Bhilai (Chhattisgarh, India). To determine the functional groups present on the magnetic bio composite surface ($Fe_3O_4$@PBP), Fourier transform infrared spectra were performed on the samples in the 4000–400 $cm^{-1}$ spectral region, the samples. FTIR spectra were acquired using an FTIR spectrophotometer (Bruker OPUS-7.5.18) based on the KBR pellet approach. The NCNR Pt. R.S.U. Raipur (C.G.) was subjected to analysis. The crystallographic compositions of $Fe_3O_4$@PBP magnetite nano composite were investigated using X-ray powder diffraction (XRD) (D8 Advance X-ray diffractometer). The sample was described using an x-ray

diffractometer and an x-ray diffraction analysis of $Fe_3O_4$@PBP in the 10–90 degree range. For X-ray detection, a Cu K-alpha tube with a wavelength of 0.154 nm from the UGC-DAE cooperation scientific research Indore was used (Bruker Lynx Eye detector).

## Adsorption analysis

Batch studies were carried out in a closed polypropylene bottle (125 ml) at a G value of 6.73 to assess the adsorption of uranium (VI) onto $Fe_3O_4$@PBP. A 50 mL concentrated solution of uranium (VI) [10–200 mg uranium (VI) /L] was prepared in which 0.01–0.3 gm of $Fe_3O_4$@PBP was added. After the batch experiment, the filtrates were collected from 5 to 70 min at equal time intervals. The pH 2–10 of sample solutions keyed with NaOH (0.1 N) was measured using a HAANA HI 5521 and HI 5522 multipara meter digital analyzer. Spectrophotometer equipment (SYSTRONICS UV–VIS spectrophotometer 117 at 651 nm) followed by the Arsenazo-III as the chromogenic agent was used to determine the concentration of uranium (VI) [27]. All studies were conducted using a magnetic stirrer (LabQuest MHS5P). Equations 1 and 2 [28] were used to compute the sorption removal efficiency (R %) and sorption capacity [$q_e$ (mg/g)] of uranium (VI) ions:

$$(R\%) = \frac{C_o - C_e}{Co} X100 \quad (1)$$

$$q_{e(\frac{mg}{g})} = \frac{C_o - C_e}{M} XV \quad (2)$$

where $C_O$ represents the initial concentration before being shaken and $C_e$ represents the final concentration of the metal ion solution [uranium (VI)] after shaking with the $Fe_3O_4$@PBP (sorbent), V (L) symbolized the volume of the metal ion solution taken for the batch adsorption trial, and M represents the mass (gm) of the $Fe_3O_4$@PBP sorbent.

## Quality assurance and quality control for applied method

Quality assurance and control strategies involve the use of certified sample solutions together with the assessment of control samples. Each measurement was carried out using only standard certified chemicals and equipment. In all tests, the standard uranium solution was employed. To ensure the reproducibility of the outcomes and data gathered, all trials in this work were carried out in triplicates. The experimental results fluctuation stayed within the estimation errors (± 10%). For precision, lab tools such as an analytical balance and a micropipette were used. The detection limit was found to be 0.025 mg/L.

## Results and discussion

### Influence of the batch operational parameters

#### Effect of pH and contact time of the solution

Figure 1a and b presented the influence of initial pH and contact time of metal ion solution on uranium (VI) sorption in batch testing at 30 °C using 0.04 gm $Fe_3O_4$@PBP added to 50 mL of uranium (VI) solution. Based on the results, pH 7 of the solution is favorable for uranium (VI) sorption by $Fe_3O_4$@PBP sorbent. At the specified pH, $Fe^{+3}$ inhibits its $OH^-$ precipitation, and may alter the interaction with $OH^-$ ions, finally achieving higher adsorption, i.e. 27.75 mg/gm [29]. The pH of the solution has an effect on the uranium (VI) species. Below pH 5, the major species is $UO_2^{+2}$, but at pH 5.0–7.0, the dominant species are $UO_2OH^+$ (hydrolysis complexes) and $(UO_2)_3(OH)_5^+$ (multinuclear hydroxide complexes) Fig. 1e. The improvement in uranium (VI) adsorption when pH rises up to pH = 7 can be explained by reducing competition for surface areas between proton and uranium (VI). When the pH exceeds 7, the removal efficiency decreases (from 88.8–40.4%) leading to the formation of $UO_2CO_3$, [$(UO_2)$, $(CO_3)_2^{2-}$], [$(UO_2)$, $(CO_3)_3^{4-}$ (carbonate uranyl ions)] and the charge of uranium (VI) species shifting from positive to negative. [30]. However, during the initial contact span time, the sorption rate was rapid and increased until it reached equilibrium (19.75–27.75 mg/gm). This is because most uranium (VI) binds to the sorbent ($Fe_3O_4$@PBP) at the beginning of the sorption process. On another end the equilibrium indicates that the uranium (VI) adsorption curves against time (min.) are relatively smooth, implying that uranium (VI) is likely encased in a monolayer on the surface of the $Fe_3O_4$@PBP [31]. The optimal removal efficiency of uranium (VI) was achieved at an initial pH of 7 in 40 min of contact span time for $Fe_3O_4$@PBP, as shown in Fig. 1 (b).

#### Effect of initial uranium (VI) concentration

The efficiency of biosorption is controlled by the concentration of metal ion it is an essential factor to consider for efficient biosorption. With a uranium initial concentration of 25 mg/L, the highest adsorption capacity ($q_e$) and removal efficiency (R %) were 27.75 mg/gm and 88.8%, respectively. As a result, this (25 mg/L) concentration was preferred as optimal and used in further trials. Figure 1c depicts the variation in removal efficiency with varying metal ion concentrations (10–200 mg/L). The amount of uranium (VI) adsorbed on the $Fe_3O_4$@PBP sorbent increased as the metal ion concentration increased (from 10 to 25 mg/L). However, as the metal ion concentration increased up to 200 mg/L,

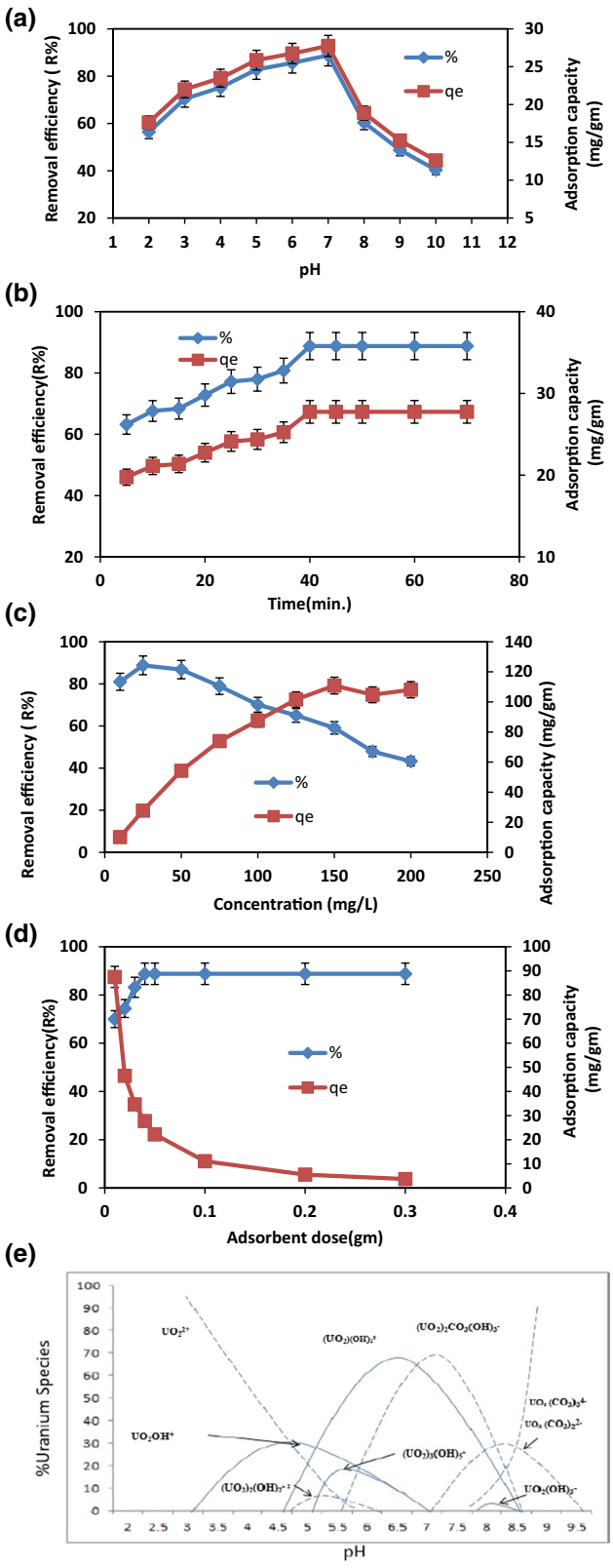


**Fig. 1** **a** Effect of the pH onto $Fe_3O_4$@PBP composite surface for uranium (VI) sorption concentration = 25 mg/L; temperature = 30; time = 40 min.; $Fe_3O_4$@PBP composite dose 0.04 gm. **b** Effect of contact time onto $Fe_3O_4$@PBP composite surface for uranium (VI) sorption concentration = 25 mg/L; temperature = 30 °C; pH = 7; $Fe_3O_4$@PBP composite dose 0.04 gm. **c** Effect of the metal ion concentration onto $Fe_3O_4$@PBP composite surface for uranium (VI) Sorption, temperature = 30 °C; pH = 7; time = 40 min.; $Fe_3O_4$@PBP composite dose 0.04 gm. d Effect of $Fe_3O_4$@PBP composite dose onto uranium (VI) sorption temperature = 30 °C; pH = 7; time = 40 min.; concentration = 25 mg/L. **e** uranium species under different pH condition

the percentage removal steadily declined to 43.25% due to saturation of the $Fe_3O_4$@PBP reactive sites. Raising the concentration of uranium in the solution is supposed to boost $q_e$ until biomass saturation ($Fe_3O_4$@PBP) is reached. With a concentration of 25 mg/L, the optimal value of $q_e$ (27.75 mg/g) was recorded. This is attributed to binding site saturation and an increase in the number of ions hoping for available reactive sites in the biomass ($Fe_3O_4$@PBP) for uranium binding at 25 mg/L concentration [32, 33]. Furthermore, higher metal ion concentrations increase mass transfer driving force and metal ion adsorption per unit mass of sorbent ($Fe_3O_4$@PBP) [34]. "Many studies show that the adsorption increases with increasing initial adsorbate (uranium) concentration and vice versa. If we reduce the adsorbate concentration further below 10 mg/L, as a concern for drinking water, adsorption would drop, but it would still be on the higher side, indicating that applied adsorbent is significant for adsorbing the uranium at low concentrations as well."

## Effect of adsorbent dosage ($Fe_3O_4$@PBP)

The sorbent dose is an important aspect to consider for effective uranium (VI) ion sorption. It determines the system's sorbent ($Fe_3O_4$@PBP) sorbate (uranium VI) balance. The number of binding sites adaptable for sorption is also determined by the amount of sorbent ($Fe_3O_4$@PBP) introduced to the uranium (VI) solution. The effect of $Fe_3O_4$@PBP dosage on uranium (VI) adsorption was investigated using varied dosages ranging from 0.01 to 0.3 gm, whereas other sorption parameters (pH, initial metal ion concentration, contact span time, and temperature) were held constant. Figure 1 d depicts the relationship between biosorption capacity ($q_e$) and percent removal (R %) with biomass ($Fe_3O_4$@PBP) concentration. As per the findings, boosting the adsorbent mass from 0.04–0.3 gm reduced the biosorption capacity from 27.75 to 3.7 mg/g. Despite the fact that the majority of functional groups on the sorbent surface available for metal ion binding increases with sorbent dosage, the results of this investigation indicated the reverse tendency. Since the $Fe_3O_4$@PBP magnetic bio-composite particles agglomerated or clustered when the sorbent mass was increased, the binding capacity for uranium ions was reduced as the sorbent mass was increased. Similar findings were found in the research of Saleem et al. and Kausar et al. [34, 35]. The same results were found in the investigations

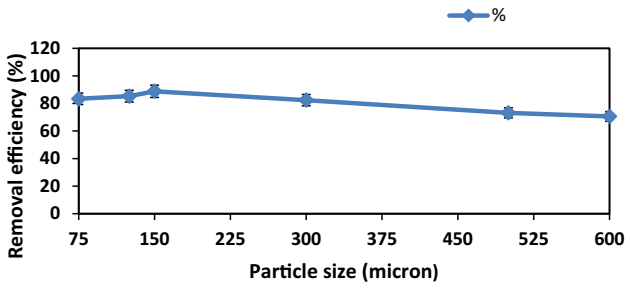


**Fig. 2** Effect of particle size onto uranium (VI) sorption, temperature = 30 °C; pH = 7 time = 40 min.; concentration = 25 mg/L; $Fe_3O_4$@PBP composites dose 0.04 gm

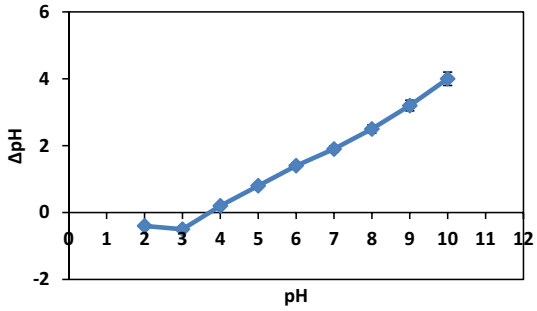


**Fig. 3** Zero point charge ($pH_{ZpC}$); pH = 2–10 of the $Fe_3O_4$@PBP composite

of Nuhanovi et al. and Šabanović et al.,who employed Sugar beet and Lemon beet as agricultural waste for uranium sorbent material [36, 37]). In all of the experiments mentioned, the optimal removal of uranium (VI) ions was accomplished with the least amount of bio sorbent mass ($Fe_3O_4$@PBP) utilized, i.e. 0.04 gm. As a result, 0.04 gm/50 mL was considered the best mass/volume ratio in further trials.

## The effect of nanocomposite particle sizes on uranium (VI) adsorption

Variations in the adsorbent ($Fe_3O_4$@PBP) grain size can affect its physiochemical properties. [38].To change the particle size, the adsorbent ($Fe_3O_4$@PBP) was sieved through several meshes, ranging from 75–600 micron (specifically 75, 125, 150, 300, 500, and 600 µm). The findings demonstrate that uranium (VI) was extracted 88.8% through the 150 micron sorbent size (Fig. 2). The findings are interesting because adsorption is normally proportional to the surface area therefore increasing particle size is expected to cause greater adsorption. But here opposite trend was observed that uranium (VI) adsorption was better at smaller sizes of particles (i,e. 150 µm). As an outcome, the size of the nanoparticles utilized in the research protocol as the sorbent was kept at 150 µm.

## Zero point charge ($pH_{ZpC}$)

Metal adsorption is primarily a pH-dependent action; adsorption equilibrium was attained in this investigation at pH 7. This behavior can be understood by the $Fe_3O_4$@PBP zero point charge (pHzpc), which was reported to be at pH 3.9 (Fig. 3). The $H^+$ ions successfully raced with the uranyl ion, resulting in less adsorption at pHzpc. However, when the pH of the $Fe_3O_4$@PBP exceeded pHzpc, the surface of the sorbent became negatively charged and electrostatically adsorbed the positively charged uranyl ions. Similar findings have been found for mango peel and banana peel [39, 40]. With increasing pH, the % removal of the $Fe_3O_4$@PBP adsorbent increased. The minimal concentration of uranyl ion uptake by the $Fe_3O_4$@PBP sorbent at lower pH levels could be caused by an increase in the concentration of hydrogen ($H^+$) ions, which fight for receptors on the adsorbent mass with uranyl ions. As the pH drops, the maximum surface charge on $Fe_3O_4$@PBP becomes positive, preventing positively charged metal cations from approaching. There is a net negative charge on the surface of $Fe_3O_4$@PBP at pH levels above the isoelectric point, and the ionic point of ligands such as carboxyl, hydroxyl, and amino groups are free to facilitate contact with metal cations. The adsorbent's metal absorption capacity ($q_e$) is determined by its nature and its pH and/ or the $pH_{PZC}$ of $Fe_3O_4$@PBP (i.e. 3.9).

## Equilibrium isotherm study

The most extensively utilized Langmuir [41] and Freundlich isotherm [42] models were employed to model equilibrium data (Fig. 4a and b). According to the Langmuir model, the maximal monolayer adsorption capacity, ($q_{max}$ mg/g), as well as other characteristics were determined by the following equation:

$$\text{Langmuir[41]}: \frac{1}{Q_e} = \left(\frac{1}{K_L Q_{max}}\right)\frac{1}{C_e} + \frac{1}{Q_{max}} \tag{3}$$

$$R_L = \frac{1}{1 + K_L c_0} \tag{4}$$

where $C_e$ denotes the equilibrium / final concentration of the uranium (VI) solution and $K_L$ represents the adsorption constant for Langmuir whereas, in Eq. 5, $q_e$ (mg/g) is the heterogeneous adsorption capacity of $Fe_3O_4$@PBP for uranium (VI) was computed using the Freundlich isotherm equation:

$$\text{Freundlich[42]}: \log Q_e = \log K_F + \frac{1}{n}\log C_e \tag{5}$$

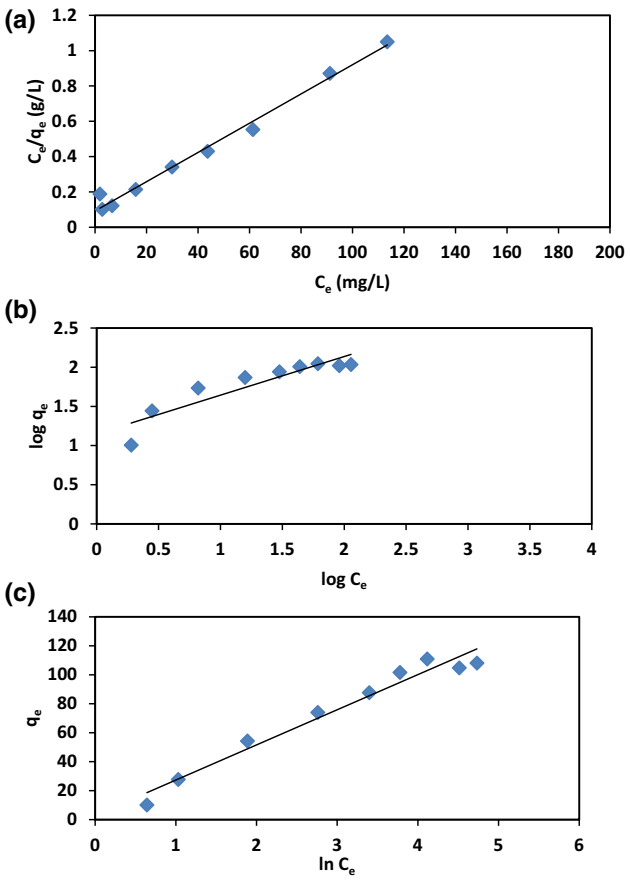


**Fig. 4** **a** Langmuir sorption model of uranium (VI) onto $Fe_3O_4$@PBP. **b** Freundlich sorption model of uranium (VI) onto $Fe_3O_4$@PBP. **c** Temkin sorption model of uranium (VI) onto $Fe_3O_4$@PBP

The heat of the sorption process is demonstrated by calculating the parameter $b_T$ (J/mol), depicted in Eq. 6 which comes from the Temkin model as shown in Fig. 4c

$$\text{Temkin}[43]: Q_e = \left(\frac{RT}{b_T}\right)\ln(A_T) + \left(\frac{RT}{b_T}\right)\ln(C_e) \quad (6)$$

The information was obtained experimentally and optimally fits to the Langmuir adsorption isotherm ($r^2 = 0.988$). It also reveals a good agreement with Temkin's model ($r^2 = 0.965$) as shown in Table 1. The computed $R_L$ value from Langmuir's calculation was within the 0–1 range, indicating that the investigated sorption is favorable. The $K_L$ value for this isotherm, in contrast is low, indicating that $Fe_3O_4$@PBP adsorbent has a strong affinity for metal ions, leading to the high adsorption of uranium (VI) to nanocomposite surfaces. Further to deduce the nature of adsorption caused physically can be attributed to weak van der Waals forces, due to which the uranium (VI) ion complexes are in harmony with the $Fe_3O_4$@PBP adsorbent surfaces. Hence this action is associated with decreased adsorption energy [44].

## Equilibrium kinetic study

To explore the process of biosorption, kinetic data were used to fit the first-order Lagergren model [45], a pseudo-second-order model [46], and a Weber and Morris model (intraparticle diffusion) [47] model. The governing equations for the corresponding models are written as follows:

$$\text{Pseudo}-\text{firstordermodel}[45]: \ln(q_e - q_t) = \ln q_e - k_1 \cdot t \quad (7)$$

$$\text{Pseudo}-\text{secondordermodel}[46]: \frac{t}{q_t} = \frac{1}{k_2 q_e^2} + \frac{1}{q_e} \cdot t \quad (8)$$

$$\text{Intraparticlediffusionmodel}[47] q_t = k_{int} \cdot t^{\frac{1}{2}} + C \quad (9)$$

where $q_e$ = adsorption capacity (mg/g) at equilibrium $q_t$ = adsorption capacity (mg/g) at time (t) $k_1$ = pseudo first-order constant (per min.) $k_2$ = pseudo second order constant (g/mg $min^{-1}$) $k_{int}$ = rate constant (mg/g·$min^{-1/2}$) of intraparticle diffusion model C = constant related to the thickness of the boundary layer (mg/g).

Figure 5a, b and c represents the adoption of alternative kinetic models to uranium sorption by $Fe_3O_4$@PBP biomass suggests that uranium sorption by $Fe_3O_4$@PBP biomass follows the pseudo second-order model (0.996), which represent that uranium adsorption is proportional to the square of unoccupied biomass sites. The value of $q_e$ (26.66) comes from the pseudo-second-order model is quite near to the experimental $q_e$ value (27.75), whereas the value obtained from the pseudo-first-order model was quite small (10.19) which is shown in Table 2.

According to the pseudo-second-order model, chemisorption controls the adsorption rate by sharing or exchanging electrons between the sorbent ($Fe_3O_4$@PBP) and sorbate (uranium VI). As an outcome, the pseudo-second-order kinetics adsorption process should be impacted by a chemical process [48].

**Table 1** Isotherm (Langmuir, Freundlich and Temkin) parameters for sorption of uranium (VI) onto $Fe_3O_4$@PBP

| Langmuir's model | | | Freundlich's model | | | Temkin's model | | |
|---|---|---|---|---|---|---|---|---|
| $K_L$ (L/mg) | $Q_{max}$ (mg/g) | $r^2$ | $K_F$(mg/g) / (mg/L) | n | $r^2$ | $A_T$ (L/g) | $b_T$ (J/mol) | $r^2$ |
| 0.0897 | 120.48 | 0.988 | 14.13 | 2.02 | 0.832 | 1.133 | 103.809 | 0.965 |

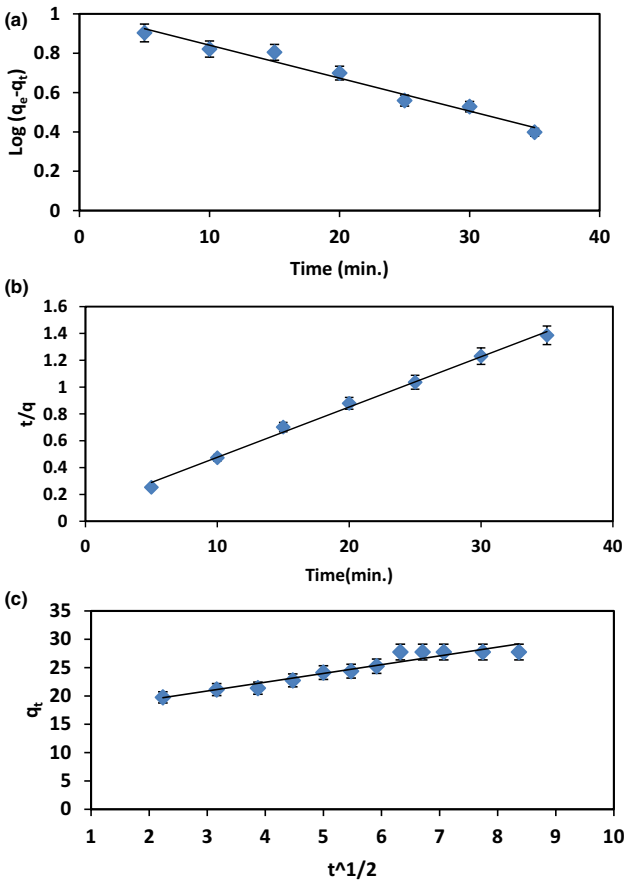


**Fig. 5** **a** Pseudo-first order kinetics for uranium (VI) sorption onto $Fe_3O_4$@PBP. **b** Pseudo-second order kinetics for uranium (VI) sorption onto $Fe_3O_4$@PBP. **c** Intra particle diffusion kinetics for uranium (VI) sorption onto $Fe_3O_4$@PBP

## Temperature influence and thermodynamic modeling

The influence of temperature on the sorption capacity of $Fe_3O_4$@PBP biomass was investigated at temperatures ranging from 25 to 40 °C, with the findings displayed in Fig. 6. As seen in the figure, the sorption capacity increased with increasing temperature, showing that uranium (VI) sorption on $Fe_3O_4$@PBP biomass was endothermic. At 30 °C, the optimal sorption capacity (27.75 mg/g) was observed. Thermodynamic aspects are used in adsorption tests to assess the spontaneity and feasibility of these processes. As an outcome, test results from the sorption process are used to

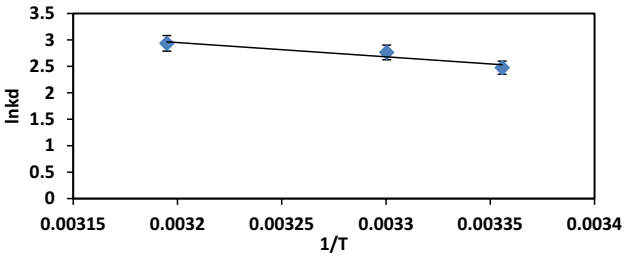


**Fig. 6** Plot of ln Kd versus t^1/2 for uranium (VI) sorption onto $Fe_3O_4$@PBP

derive thermodynamic parameters such as Gibbs free energy ($\Delta G^0$), enthalpy ($\Delta H^0$), and entropy ($\Delta S^0$), as shown in the equation.

$$\ln K_d = -\frac{\Delta H^\circ}{RT} + \frac{\Delta S^\circ}{R} \tag{10}$$

$$\Delta G^\circ = \Delta H^\circ - T\Delta S^\circ \tag{11}$$

where $K_d$ (L/g) = distribution coefficient R (kJ/mol·K) = gas constant ($8.314 \times 10^{-3}$) T (K)) = temperature.

Table 3 presented the values for ΔG°, ΔH°, and ΔS° for uranium (VI) sorption, with the negative ΔG° demonstrating that the adsorption mechanism is spontaneous. A positive ΔH° value means that the adsorption path is endothermic, and positive ΔS° values explain the enhanced randomization between the solid–liquid [$Fe_3O_4$@PBP – U (VI)] boundary, revealing that the $Fe_3O_4$@PBP adsorbent has a desire for uranium (VI). Physisorption comes into play when the heat seems to be between 2.1–20.9 kJ/mol, whereas chemical adsorption arises when the heat is somewhere between 80–200 kJ/mol[49]. Sorption of uranium (VI) onto $Fe_3O_4$@PBP is thus best summed up as a physicochemical sorption process. Negative ΔG° values suggest that the examined adsorption mechanism is spontaneous since the values vary from -20 to—80 kJ/mol simultaneously.

## Desorption test

One of the most significant parts of any successful sorption process is the recovery of metal ions [uranium (VI)] trapped onto the biomass. Adsorbed metal ions should be easily separated under proper circumstances for frequent use

**Table 2** Parameters for Kinetic of uranium (VI) sorption by $Fe_3O_4$@PBP

| S.NO | Pseudo-first order | | | Pseudo-second order | | | Intraparticle diffusion model | | |
|---|---|---|---|---|---|---|---|---|---|
| $q_{exp}$ | $K_1$ (1/min) | $q_e$ (mg/g) | $r^2$ | $K_2$ (g/mg min) | $q_e$ (mg/g) | $r^2$ | $K_{int}$ | C | $r^2$ |
| 27.75 | 0.0386 | 10.19 | 0.971 | 0.0138 | 26.66 | 0.996 | 1.5486 | 16.22 | 0.920 |

**Table 3** Thermodynamic Parameters for sorption of uranium (VI) onto $Fe_3O_4$@PBP

| Temperature (K) | ΔH° (kJ/mol) | ΔS° (J/mol·K) | ΔG° (kJ/mol) |
|---|---|---|---|
| 298 | 22.435 | 96.326 | – 28.68 |
| 303 | | | – 29.16 |
| 313 | | | – 30.12 |

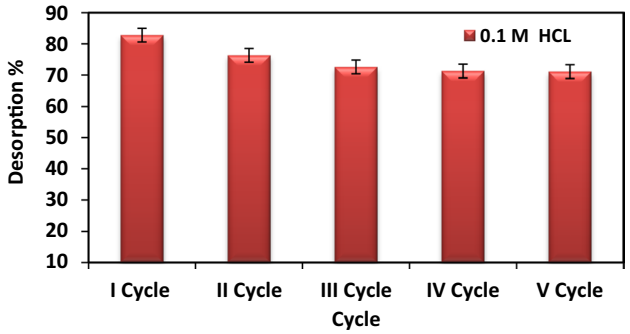


**Fig. 7** Impact of eluent on a percentage of uranium (VI) elution

**Table 4** Desorption percentage with different desorbing solution

| Desorbing solution | 0.1 M HCl | 0.1 M $CH_3COOH$ | 0.1 M EDTA | 0.1 M $NaHCO_3$ |
|---|---|---|---|---|
| Desorption percentage | 82.8 | 78.6 | 75.6 | 70.4 |

of biosorbent. Desorption is an essential phase in sorption analyses because it promotes sorption. The desorption of adsorbed uranium (VI) ions from $Fe_3O_4$@PBP biomass was tested in batch mode under ideal conditions (for 24 h). After employing several eluents (HCl, $CH_3COOH$, EDTA, and $NaHCO_3$), the findings are presented in Fig. 7. As inferred from the figure, HCl was an effective de-sorbent (82.8% desorption with 0.1 M HCl). Table 4 shows the desorption effectiveness of HCl followed by $CH_3COOH$, EDTA, and $NaHCO_3$. HCl showed great regeneration efficiency, which can be related to its ion exchange abilities. The same method was performed five times for the following adsorption–desorption cycles after optimizing the strength of the HCl solution (0.1 M). These findings indicate that the $Fe_3O_4$@PBP biomass has a high potential for periodically removing uranium ions from the aqueous phase with no noticeable reduction in total biosorption capability. The desorption efficiency was calculated using Eq. 12 (Table 5).

$$\text{Desorption\%[50]} = \frac{\text{Desorbed uranium (VI) in milligram per litre}}{\text{Adsorbed uranium (VI) in milligram per litre}} \times 100 \quad (12)$$

## Characterization analysis of $Fe_3O_4$@PBP

### Infrared study of $Fe_3O_4$@PBP

Spectral analysis in the middle-infrared region (4000–500 $cm^{-1}$) has been used to detect key functional groups often during U(VI) adsorption on the $Fe_3O_4$@PBP composite (Figs. 8a and b). As a matter of fact, the sorption of target ions over $Fe_3O_4$@PBP composite is reflected in an alteration in FTIR peak values. The broad peak at 3351.07 $cm^{-1}$ for $Fe_3O_4$@PBP adsorbent is ascribed to OH stretching vibrations of phenols, alcohols, and carboxylic acids on the spectrum upon adsorption (3236.80 $cm^{-1}$). The asymmetric and symmetric stretching vibrations of -C = O groups are responsible for the peak at 1614.39 $cm^{-1}$, which is slightly moved to 1615.48 $cm^{-1}$ further to adsorption. Spectrum peaks in the 580–625 $cm^{-1}$ range could be assigned to $Fe_3O_4$

**Table 5** Maximum sorption capacity from the earlier work compared to present results

| S.No | Sorbent | Optimal Temp | Optimal pH | Maximum adsorption capacity (qmax) | References |
|---|---|---|---|---|---|
| 1 | GO-CTS | 298 K | 5 | 50.51 mg/g | [53] |
| 2 | Oxidized MWCNTs | 298 K | 5 | 45.9 mg/g | [54] |
| 3 | Zeolite | 293 K | 6 | 11.13 mg/g | [55] |
| 4 | Magnetic Chitosan | 298 K | 5 | 42 mg/g | [56] |
| 5 | $Fe_3O_4$@SBA-15-PDA/HBP-$NH_2$ | 298 K | 6 | 77.4 mg/g | [57] |
| 6 | CS-Ppy- $Fe_3O_4$-AO | 298 K | 6 | 3.75 mg/g | [58] |
| 7 | $Fe_3O_4$@PBP | 303 K | 7 | 120.48 mg/g | Current study |

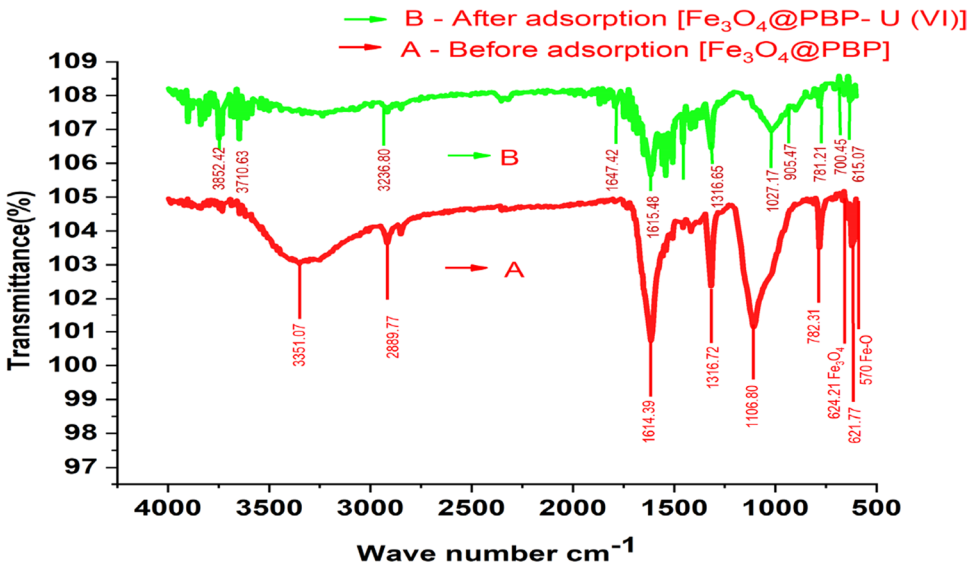


**Fig. 8** **A** and **B** FTIR spectrum of $Fe_3O_4$@PBP, **A** before uranium (VI) sorption and **B** after sorption of uranium (VI)

(Fe–O bond), indicating effective binding [51]. The FTIR analysis of the uranium ion-loaded $Fe_3O_4$@PBP composite reveals which functional groups are engaged in the sorption of the uranium ions. The bands at 2889.77, 1614.39, 1316.72, and 1106.80 $cm^{-1}$ were displaced to 3236.80, 1647.42, 1316.65, and 1027.17 $cm^{-1}$ showing that carboxyl and hydroxyl as well as N–O stretching of aromatic amines, had a role in associating uranium ions to the $Fe_3O_4$@PBP composite. FTIR study findings indicate that functionalization of uranium with carboxyl and hydroxyl group emerges in uranium (VI) binding onto $Fe_3O_4$@PBP. Furthermore, after the disappearance of an IR band, such as the band at 570 $cm^{-1}$, an extra peak at 905 $cm^{-1}$ is seen and can be referred to as the U–O bond [52]. The disappearance and appearance of new bands, along with alterations in band intensity, may be believed to be due to uranium adsorption over the $Fe_3O_4$@PBP.

## Surface morphology and elemental (SEM–EDX) study of $Fe_3O_4$@PBP

The SEM imaging of unloaded uranium (VI), $Fe_3O_4$@PBP sorbent (Fig. 9a) and loaded uranium (VI), $Fe_3O_4$@PBP sorbent (Fig. 9b) demonstrate the difference in surface morphology. The surface morphology of unloaded uranium (VI) $Fe_3O_4$@PBP sorbent was cavity whereas that of loaded uranium (VI) $Fe_3O_4$@PBP sorbent was porous. The porous structure of the loaded uranium (VI) $Fe_3O_4$@PBP adsorbent, as demonstrated by SEM, renders the composite suitable as an adsorbent. There is heterogeneity prior to adsorption

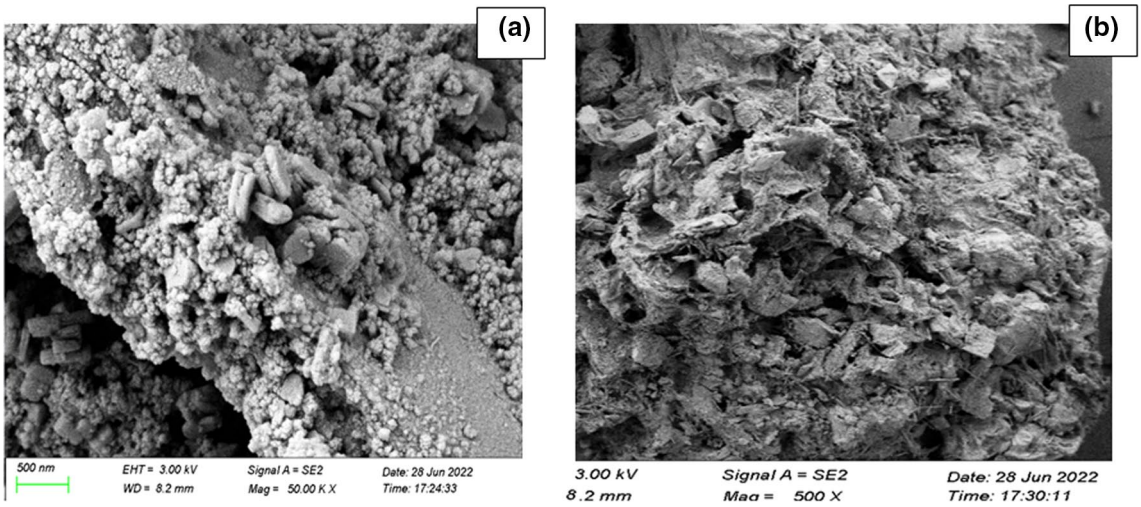


**Fig. 9** **a** and **b** SEM morphology of $Fe_3O_4$@PBP **a** before uranium (VI) sorption and **b** after sorption of uranium (VI)

that adjusts upon adsorption due to basically round and/or spherical surface morphologies. An EDX (Energy Dispersive Spectroscopy) of the proposed adsorbent material, namely $Fe_3O_4$@PBP adsorbent, proves the presence of Ca, C, Cl, Fe, P, Na, and O elements. One of the most important analytical techniques for determining the elemental content of materials is EDX (Fig. 10a and b). Analyzing the EDX spectra of the $Fe_3O_4$@PBP adsorbent composite obtained after the remediation investigation indicated the extraction of uranium (VI) (Fig. 10b). Meanwhile, an extra uranium (VI) peak is clearly evident on the uranium (VI) laden $Fe_3O_4$@PBP adsorbent. The action of an X-ray source with objects is defined.

### XRD analysis of $Fe_3O_4$@PBP composite

Co-precipitation was implemented to produce $Fe_3O_4$@PBP nano biocomposites. The particle sizes of such composite ($Fe_3O_4$@PBP) were computed by using the Debye-Scherer equation. As illustrated in Fig. 11, the XRD pattern of $Fe_3O_4$@PBP was matched to the usual JCPDS data for peak indexing (JCPDS 85–1436). The diffraction pattern was seen to be similar to the cubic phase of the $Fe_3O_4$@PBP pattern exhibiting different peaks at 2θ. As a result, the XRD pattern obviously shows the sorbent's $Fe_3O_4$ contents. Diffraction peaks demonstrate the exceptional crystallinity of $Fe_3O_4$ at 2 θ (in the range of 10–90°). The XRD spectra showing several peaks at 2θ values of 16.54°, 29.74°, 35.7°, 43.42°, 57.6°, and 63.10° are corresponding to (111)c, (220)c, (311)c, (400)c, (511)c, and (440)c orientations of $Fe_3O_4$, as well as other minor peaks. The most desired orientation was observed to be at $29.64^0$, which closely matched the most intense peak of $Fe_3O_4$ shown to be at $35.44^0$ for the (311)c peak. As a result, the X-ray diffraction analysis clearly support the presence of $Fe_3O_4$.

Using XRD, Eq. 13 is applied to determine the particle size of a material. The average particle size of magnetic particles in the XRD peak is 26.4 nm.

$$D = \frac{k\lambda}{\beta\cos\theta} \tag{13}$$

where D and $\lambda$ = average crystalline size and wavelength of the X-ray used. k = Scherrer constant (approximately 0.9). $\beta$= intensity in angular line (FWHM), $\theta$= Bragg angle.

## Mechanism

Green synthesis of nanoparticles employs a bottom-up approach in which metal atoms form clusters and, eventually, nanoparticles. The biological components of green materials may serve also as reducing and capping agents, enabling the stabilization of nanoparticles during the synthesis process. This enables you to alter the surface morphology (via. size and shape) of the nanoparticles, which can therefore be used in a variety of ways. It's indeed to grasp the basic adsorption behavior for the removal of target metals (uranium VI) from samples taken (Water). Not just do surface properties, functional groups and the appropriate arrangement of sorbent

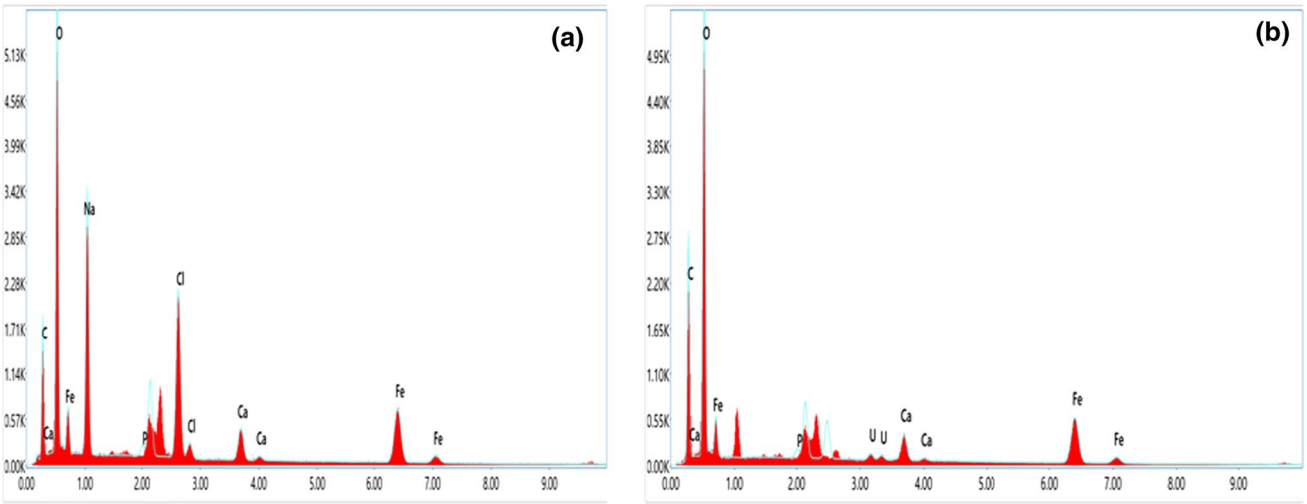


**Fig. 10** **a** and **b** EDX spectrum of $Fe_3O_4$@PBP **a** before uranium (VI) sorption and **b** after sorption of uranium (VI)

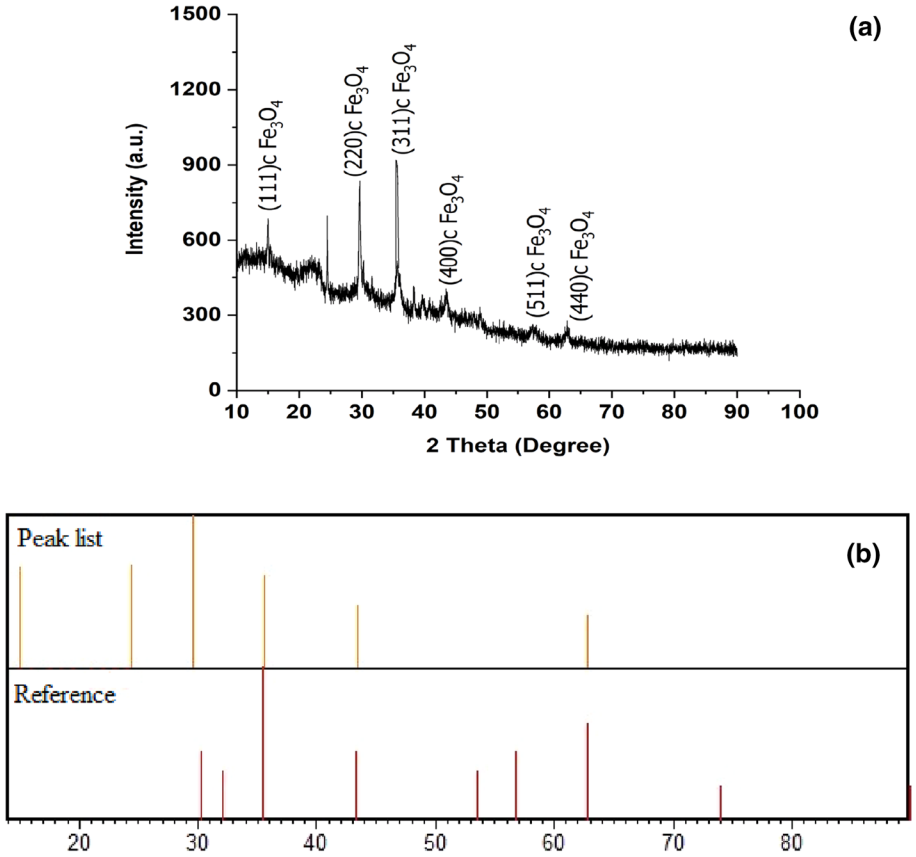


**Fig. 11** **a** XRD pattern of $Fe_3O_4$@PBP composite **b** Peak with standard reference

($Fe_3O_4$@PBP) materials influence the mechanism, but also the type of target metal ion (uranium VI). When $Fe_3O_4$@PBP was used as a sorbent to adsorb uranium (VI), interactions such as physical adsorption, ion exchange, and electrostatic attraction were observed. On the surface of $Fe_3O_4$@PBP composite, uranium (VI) ions are likely associated with nitrogen or oxygen of electron-dense functional [i.e. carboxylic (-COOH), hydroxyl ($OH^-$) and amine ($NH_2^-$)]. $Fe_3O_4$@PBP composite has Fe-OH groups on their surfaces. All above group also deprotonates when pH upturn and protonates further since pH drops. As an outcome, adjusting the pH of the solution directly impacts the acceptance or disgust of uranium (VI). Along with oxygen, the principal cooperation in the optimal pH range is metal–ligand chelation. When the SEM–EDX patterns of produced $Fe_3O_4$@PBP in the loaded and unloaded uranium (VI) were compared, it was noted that loaded uranium (VI) into the sorbent surface of ($Fe_3O_4$@PBP) clearly exhibited alterations in their surface morphology (Fig. 9a and b). In this investigation, the occurrence of carboxylic, hydroxyl, and amine groups in FTIR spectra (Fig. 8a and b) was mostly relevant for the sorption of uranium (VI). The XRD spectrum was employed to identify phase transparency and the most significant peak in the $Fe_3O_4$@PBP XRD profile, as shown in Fig. 11.

## Conclusion

The $Fe_3O_4$@PBP composite showed potential as a suitable adsorbent for aqueous uranium (VI) removal. The adsorption of uranium (VI) onto $Fe_3O_4$@PBP composite particles was significantly enhanced by increasing the pH. The optimum adsorption effect was attained at pH 7. Successful adsorption of uranium (VI) from an aqueous solution was achieved, with a maximum sorption capacity of 120.48 mg/g at 30 degrees Celsius. It took only 40 min for the sorption equilibration to reach equilibrium. Uranium sorption can be perfectly described by the Langmuir isotherm model. Additionally, the study's key findings provide a way to remove metal ions from water. Moreover, the pseudo-second-order kinetics was closely matched to the results for the $Fe_3O_4$@PBP composite. Sorption of uranium (VI) has been confirmed to be endothermic and to take place spontaneously, according to thermodynamic studies. These $Fe_3O_4$@PBP composites proved effective Scavengers for extracting uranium (VI) from metal-containing water, as evidenced by the removal of the ion from the solution. $Fe_3O_4$@PBP nanocomposites were thoroughly analyzed using XRD, FT-IR, FE-SEM, and EDX. Green synthesis, as employed in this study, avoids the need for potentially dangerous chemicals, and expanding the operation is easy and cheap.

**Acknowledgements** The authors would like to acknowledge the Principal of BIT Durg (C.G.) for providing lab facilities. The authors are grateful to the NCNR, Pt.R.S.U. Raipur for offering FTIR facilities, as well as IIT Bhilai and the UGC-DAE consortium for scientific research Indore for providing SEM, EDS, and XRD facilities.

**Funding** This research was not funded in any way.

## Declarations

**Conflict of interest** There are no relevant financial interests to disclose for the authors.

## References

1. Liu N, Li C, Bai J, Liang H, Gao Q, Wang N, Guo R, Qin Z, Zunli M (2021) A high-capacity amidoxime-functionalized magnetic composite for selective uranium capture in salt lake water. J Environ Chem Eng. https://doi.org/10.1016/j.jece.2021.106688
2. Bjørklund G, Semenova Y, Pivina L, Dadar M, Rahman MM, Aaseth J, Chirumbolo S (2020) uranium in drinking water: a public health threat. Arch Toxicol. https://doi.org/10.1007/s00204-020-02676-8
3. WHO (2011) Guidelines for drinking water quality. 4th ed. WHO Press: Geneva, Switzerland
4. Tuzen M, Saleh TA, Sar A, Sar N (2020) Interfacial polymerization of trimesoyl chloride with melamine and palygorskite for efficient uranium ions ultra-removal. Chem Eng Res Des. https://doi.org/10.1016/j.cherd.2020.04.034
5. Saleh TA, Naeemullah Tuzen M, Ahmet S (2017) Polyethylenimine modified activated carbon as novel magnetic adsorbent for the removal of uranium from aqueous solution. Chem Eng Res Des. https://doi.org/10.1016/j.cherd.2016.10.030
6. Wang Z, Hu H, Huang L, Lin F, Liu S, Wu T, Wang X, Rabah SO, Lu Y, Wang X (2020) Graphene aerogel capsulated precipitants for high efficiency and rapid elimination of uranium from water. Chem Eng J. https://doi.org/10.1016/j.cej.2020.125272
7. Tapia-Rodriguez A, Luna-VelascoA FJA, Sierra-Alvarez R (2010) Anaerobic bioremediation of hexavalent uranium in groundwater by reductive precipitation with methanogenic granular sludge. Water Res. https://doi.org/10.1016/j.watres.2009.12.030
8. He M, Wang L, Zhang Z, Zhang Y, Zhu J, Wang X, Miao R, Miao R (2020) Stable forward osmosis nanocomposite membrane doped with sulfonated graphene oxide@metal–organic frameworks for heavy metal removal. ACS Appl Mater Interfaces. https://doi.org/10.1021/acsami.0c17405
9. Cecal A, Humelnicu D, Rudic V, Cepoi L, Ganju D, Cojocari A (2012) Uptake of uranyl ions from uranium ores and sludges by means of spirulina platensis, porphyridium cruentum and nostok linckia alga. Bioresour Technol. https://doi.org/10.1016/j.biortech.2012.05.053
10. Tan L, Zhang X, Liu Q, Jing X, Liu J, Song D, Wang J, Liu L, Wang J (2015) Synthesis of $Fe_3O_4$@TiO2 core–shell magnetic composites for highly efficient sorption of uranium(VI). Colloids Surf A. https://doi.org/10.1016/j.colsurfa.2015.01.040
11. Yu B, Xu J, Liu JH, Yang ST, Luo J, Zhou Q, Liu Y, Liao R, Wang H, Liu Y (2013) Adsorption behavior of copper ions on graphene oxide–chitosan aerogel. J Environ Chem Eng. https://doi.org/10.1016/j.jece.2013.08.017
12. Duan X, Zhang C, Srinivasakannan C, Wang X (2017) Waste walnut shell valorization to iron loaded biochar and its application to arsenic removal. Resour-Effic Technol 3:29–36
13. Han C, Li H, Pu H, Yu H, Deng L, Huang S, Luo Y (2013) Synthesis and characterization of mesoporous alumina and their performances for removing arsenic (V). Chem Eng J 217:1–9
14. Ren Z, Zhang G, Paul Chen J (2011) Adsorptive removal of arsenic from water by an iron-zirconium binary oxide adsorbent. J Colloid Interface Sci 358:230–237
15. Ungureanu G, Santos S, Boaventura R, Botelho C (2015) Arsenic and antimony in water and wastewater: overview of removal techniques with special reference to latest advances in adsorption. J Environ Manage 151:326–342
16. Mohan D, Pittman CU (2007) Arsenic removal from water/wastewater using adsorbents-a critical review. J Hazard Mater 142:1–53
17. Kausar A, Bhatti HN (2013) Adsorptive removal of uranium from wastewater: a review. J Chem Soc Pakistan 35(3):1041–1052
18. Mohan D, Sarswat A, Singh VK, Alexandre-Franco M, Pittman CU (2011) Development of magnetic activated carbon from almond shells for trinitrophenol removal from water. Chem Eng J 172:1111–1125
19. Kashyap Agarwal A (2019) Removal of salicylic acid from aqueous solutions by magnetic bio sorbent synthesized from pineapple peel. J Pharm Innov 8:502–504
20. Dick G (2003) Papaya: A tantalising taste of the tropics. maricopa county master gardener volunteer information, University of Arizona Cooperative Extension
21. Shaik Basha ZVP, Murthy Jha B (2008) Sorption of Hg (II) from aqueous solutions onto carica papaya: application of isotherms. Ind Eng Chem Res 47:980–986
22. Saeed A, Akhter MW, Iqbal M (2005) Removal and recovery of heavy metals from aqueous solution using papaya wood as a new biosorbent. Sep Purif Technol. https://doi.org/10.1016/j.seppur.2005.02.004
23. Li X, Xu H, Chen ZS, Chen G (2011) Biosynthesis of NPs by microorganisms and their applications. J Nanomater. https://doi.org/10.1155/2011/270974
24. Naeem H, Bhattia HN, Sada S, Iqbal M (2017) Uranium remediation using modified vigna radiata waste biomass. Appl Radiat Isot 123:94–101
25. Igwegbe WE, Okoro BC, Osuagwu JC (2015) Use of carica papaya as a bio- sorbent for removal of heavy metals in waste water. Int Scholarly Sci Res Innov 9(12):1400–1404
26. Daoush WM (2017) Co-precipitation and magnetic properties of magnetite nanoparticles for potential biomedical applications. J Nanomed Res 5(3):1–12
27. Srivastava PK (2016) Spectrophotometric analysis of underground well water uranium of an abondon coal mines. IOSR J Environ Sci Toxicol Food Technol 10:101–105
28. Yuan Y, Liu N, Dai Y, Wang B, Liu Y, Chen C, Huang D (2020) Effective biosorption of uranium from aqueous solution by cyanobacterium anabaena flos-aquae. Environ Sci Pollut Res Int 27(35):44306–44313
29. Wang S, Guo W, Gao F, Wang Y, Gaoc Y (2018) Lead and uranium sorptive removal from aqueous solution using magnetic and nonmagnetic fast pyrolysis rice husk biochars. RSC Adv 8:13205–13217
30. Yu A, Wang J, Jiang Y (2016) Removal of uranium from aqueous solution by alginate beads. Jing Nucl Eng Technol 49:534–540
31. Rengaraj S, Moon SH, Sivabalan R, Arabindoo B, Murugesan V (2002) Removal of phenol from aqueous solution and resin manufacturing industry wastewater using an agricultural waste: Rubber seed coat. J Hazard Mater 89(2–3):185–196
32. Hanif MA, Nadeem R, Bhatti HN, Ahmad NR, Ansari TM (2007) Ni (II) bio sorption by Cassia fistula (Golden Shower) biomass. J Hazard Mater 139:345–355
33. Zubair A, Bhatti HN, Hanif MA, Shafqat F (2008) Kinetic and equilibrium modeling for Cr(III) and Cr(VI) removal from

aqueous solutions by citrus reticulate waste biomass. Wat Air Soil Pollut 191:305–318
34. Saleem N, Bhatti HN (2011) Adsorptive removal and recovery of U (VI) by citrus waste biomass. Bio Resources. https://doi.org/10.15376/biores.6.3.2522-2538
35. Kausar A, Bhatti HN (2013) Adsorptive removal of uranium from wastewater: a review. J The Chem Soc Pak 35(3):1041–1052
36. Nuhanović M, Grebo M, Draganović S, Memić M, Smječanin N (2019) Uranium (VI) biosorption by sugar beet pulp: equilibrium, kinetic and thermodynamic studies. J Radioanal Nucl Chem 322(3):2065–2078
37. Šabanović E, Muhić-Šarac T, Nuhanović M, Memić M (2019) Biosorption of uranium (VI) from aqueous solution by Citrus limon peels: kinetics, equlibrium and batch studies. J Radioanal Nucl Chem 319(1):425–435
38. Velizar S, Dragana B, Milan G, Bogdanović G (2009) Heavy metal ions adsorption from mine waters by sawdust. Chem Ind Chem Eng. https://doi.org/10.2298/CICEQ0904237S
39. Iqbal MA, Saeed Zafar SI (2009) FTIR spectrophotometry, kinetics and adsorption isotherms modeling, ion exchange, and EDX analysis for understanding the mechanism of $Cd^{2+}$ and $Pb^{2+}$ removal by mango peel waste. J Hazard Mater 164:161–171
40. Anwar J, Shafique U, Waheed Z, Salman M, Dar A, Anwar S (2010) Removal of Pb (II) and Cd (II) from water by adsorptionon peels of banana. Bioresource Technol 101:1752–1755
41. Langmuir I (1918) The adsorption of gases on plane surfaces of glass, mica, and platinum. J Am Chem Soc 40:1361–1368
42. Freundlich H (1906) Adsorption in solution Phys Chem Soc 40:1361–1368
43. Araújo CS, Almeida IL, Rezende HC, Marcionilio SM, Léon JJ, de Matos TN (2018) Elucidation of mechanism involved in adsorption of Pb (II) onto lobeira fruit (solanum lycocarpum) using langmuir, freundlich and temkin isotherms. Microchem J. https://doi.org/10.1016/j.microc.2017.11.009
44. Esfandiari B, Monajjemi M (2013) Physical adsorption between mono and diatomic gases inside of carbon nanotube with respect to potential energy. J Phys Theor Chem 10:31–42
45. Lagergren S (1898) Zur theorie der sogenannten adsorption geloster stoffe", kungligasvenska vetenkapsakademiens. Handlinger. https://doi.org/10.1007/BF01501332
46. Blanchard G, Maunaye M, Martin G (1984) Removal of heavy metals from waters by means of natural zeolites. Water Res 18:1501–1507
47. Weber WJ, Morris JC (1963) Kinetics of adsorption on carbon solution. J Sanit Eng Div A Soc Civil Eng 89:31–35
48. Pan M, Lin X, Xie J, Huang X (2017) Kinetic, equilibrium and thermodynamic studies for phosphate adsorption on aluminum hydroxide modified palygorskite nano-composites. RSC Adv 7(8):4492–4500
49. Liu Y, Liu YJ (2008) Biosorption isotherms, kinetics and thermodynamics. Sep Purif Technol 61(3):229–242
50. Yin X, Bai J, Fan F, Cheng W, Tian W, Wang Y, Zhi Qin Z (2015) Amidoximed silica for uranium (VI) sorption from aqueous solution. J Radioanal Nucl Chem. https://doi.org/10.1007/s10967-014-3652
51. Adeogun A, Akande J, Idowu M, Kareem S (2019) Magnetic tuned sorghum husk biosorbent for effective removal of cationic dyes from aqueous solution: isotherm, kinetics, thermodynamics and optimization studies. Appl Water Sci 9:1–17
52. Cheng Y, Li F, Liu N, Lan T, Yang Y, Zhang T, Qing R (2021) A novel freeze-dried natural microalga powder for highly efficient removal of uranium from wastewater. Chemosphere. https://doi.org/10.1016/j.chemosphere.2021.131084
53. Yang A, Yang P, Huang CP (2017) Preparation of graphene oxide–chitosan composite and adsorption performance for uranium. J Radioanal Nucl Chem. https://doi.org/10.1007/s10967-017-5329-4
54. Schierz A, Zänker H (2009) Aqueous suspensions of carbon nanotubes: surface oxidation, colloidal stability and uranium sorption. Environ Pollut. https://doi.org/10.1016/j.envpol.2008.09.045
55. Zou W, Bai H, Zhao L, Li K, Han R (2011) Characterization and properties of zeolite as adsorbent for removal of uranium (VI) from solution in fixed bed column. J Radioanal Nucl Chem. https://doi.org/10.1007/s10967-011-1026-x
56. Stopa LCB, Yamaura M (2010) Uranium removal by chitosan impregnated with magnetite nanoparticles: adsorption and desorption. Int J Nucl Energy Sci and Technol. https://doi.org/10.1504/IJNEST.2010.035538
57. Liu F, Wang A, Xiang M, Hu Q, Hu B (2022) Effective adsorption and immobilization of Cr (VI) and U (VI) from aqueous solution by magnetic amine-functionalized SBA-15. Sep Purif Technol. https://doi.org/10.1016/j.seppur.2021.120042
58. Liu L, Lin X, Li M, Chu H, Wang H, Xie Y, Luo X, Liu M, Liang L, Gong H (2021) Microwave-assisted hydrothermal synthesis of carbon doped with phosphorus for uranium (VI) adsorption. J Radioanal Nucl Chem. https://doi.org/10.1007/s10967-020-07453-6



## Authors and Affiliations

**Poonam Deshmukh[1] · Santosh Kumar Sar[1] · Manoj Kumar Jindal[1,3] · Tonmoy Ray[2]**

✉ Poonam Deshmukh
poonamdeshmukh284@gmail.com

Santosh Kumar Sar
santosh.sar@bitdurg.ac.in

Manoj Kumar Jindal
manojjindal1989@gmail.com

Tonmoy Ray
ray-tonmoy96@g.ecc.u-tokyo.ac.jp

[1] Department of Applied Chemistry, Bhilai Institute of Technology, Durg 491001, India

[2] Aida Lab, Department of Chemistry and Biotechnology, School of Engineering, The University of Tokyo, Tokyo, Japan

[3] Divecha Centre for Climate Change, Indian Institute of Science, Bangalore, India